Journal of Machine Engineering, 2024, Vol. 24, No. 1, 118–134
ISSN 1895-7595 (Print) ISSN 2391-8071 (Online)

Received: *06. February. 2024* / Accepted: *10 March 2024* / Published online: *13 March 2024*

ultra-precision machining, circulating abrasive flow, magneto-rheological finishing, circular Halbach array, Ti-6Al-4V

Nguyen Duy TRINH[1], Dung Hoang TIEN[1*], Pham Thi Thieu THOA[1], Nguyen Van QUE[1], Kieu Van QUANG[2], Nguyen Trong MAI[1], Nguyen Ngoc QUAN[1], Ngo Minh NHAT[3]

A NOVEL CIRCULATING ABRASIVE FLOW STRATEGY USING CIRCULAR HALBACH ARRAY FOR MAGNETO-RHEOLOGICAL FINISHING OF Ti-6Al-4V

In the pursuit of advancing the surface machining efficiency of Ti-6Al-4V material through magnetic polishing, this study introduces a new approach methodology. A novel approach integrates Magneto-Rheological Finishing (MRF) into a circulating system, employing a circular Halbach array to ensure a continuous and uniform flow of magnetic abrasives. Employing simulation and theoretical analysis, MRF polishing processes with the fluid dynamics of abrasive (SiO_2) and magnetic particles (Fe_3O_4) during the finishing process of Ti-6Al-4V material using a circulating conveyor designed for the regeneration of abrasive particles. To investigate the impact of magnetic fluid distributions influenced by magnetic fields on the machining process, we meticulously conduct experimental analyses. The findings underscore that diminishing the working distance results in an expanded distribution range of magnetic abrasive fluid on the conveyor belt. Consequently, this induces a noteworthy variation in impact positions on the workpiece surface, leading to an increased exposed area. A pivotal outcome of this study is the observed augmentation in machining quality and efficiency. Remarkably, the surface roughness of the Ti-6Al-4V workpiece undergoes a substantial improvement, diminishing from an initial *Ra* = 431.1 nm to an impressive *Ra* = 39.6 nm within a 30-minute timeframe.

1. INTRODUCTION

With the escalating demand for heightened precision, conventional techniques such as grinding and polishing often fall short of achieving nanometer precision and surface smoothness on advanced engineering materials. As a result, the integration of magnetic fields into the production process has garnered significant attention within the scientific community. The explored Magneto-Rheological Finishing (MRF) has emerged as a pivotal contributor to the advancement of high-tech industries, including aerospace, mould polishing, semicon-

[1] Faculty of Mechanical Engineering, Hanoi University of Industry, Hanoi city, Vietnam
[2] Vietnam-Japan Center, Hanoi University of Industry, Hanoi city, Vietnam
[3] Faculty of Mechanical Engineering, Hanoi College of High Technology, Vietnam
[*] E-mail: tiendung@haui.edu.vn
https://doi.org/10.36897/jme/185893

ductors, and other sectors necessitating exceptional precision. In the MRF process, the magnetic field within the working area generates the requisite machining force, with the machining tool (magnetic brush) incorporating magnetic particles [1–3]. This characteristic renders it flexible and easily adherent to the machined surface, positioning this process as an emerging precision machining technology with great potential [4–6]. Numerous studies have explored MRF in recent years, finding diverse applications in fields such as medical and optical part machining [7–9]. Harris et al. [10] elucidated the polishing characteristics and the material removed principle of MRF, affirming its capacity for precise finishing. Xu et al. [11] introduced an innovative approach by incorporating vibration assistance in MRF polishing to enhance effective surface finishing. Shafrir et al. [12] employed a sophisticated sol-gel process to fabricate ZrO_2-coated carbonyl-iron particles, resulting in a stable Material Removal Rate (MRR) and superior surface quality for optical glass and ceramics through MRF polishing. In the context of polishing sapphire wafers, SiO_2 emerges as a more favourable material than CeO_2 and ZrO_2. The abrasive SiO_2 exhibits preference due to its capacity to react with the sapphire surface, creating a soft layer easily removable through mechanical action, as observed in previous studies [13–15]. Pan et al. [16] innovatively developed SiO_2-CI composite particles using the sol-gel method for MRF of sapphire materials. Their findings revealed that the synthetic abrasive not only enhances the chemical reaction rate but also augments the mechanical removal rate on the sapphire surface during the polishing process. In a similar vein, Zhai et al. [17] prepared Fe_3O_4-SiO_2 composite particles for MRF of sapphire plates, leading to improved surface quality and polishing effects when compared to the use of SiO_2-CI composite abrasives. Furthermore, their study explored the correlation between sapphire MRR and the viscosity of the MRF slurry. These research endeavours contribute valuable insights to the understanding and optimization of MRF processes for diverse materials. However, it is noteworthy that the current models for MRF have not thoroughly addressed the incorporation of regenerate abrasive particles in the polishing area to always create new abrasive particles in contact with the machined surface taking advantage of the effectiveness derived from an applied magnetic field. The exploration of regenerate abrasive particle manipulation techniques within the finishing zone and the optimization of the magnetic field's impact are areas where further research could yield substantial advancements in MRF modelling and application.

Surface finishing of titanium alloys has become a focal point of research, particularly with its diverse applications in aerospace, biology, chemistry, and medicine. The distinctive characteristics of Ti alloys, such as low toxicity, exceptional corrosion resistance, commendable toughness, and high tensile and yield strength, underscore their significance [18–20]. However, machining Ti alloys poses inherent challenges due to their high chemical reactivity, low thermal conductivity, and low elastic modulus [21, 22]. Recent research efforts have focused on utilizing MRF polishing to improve surface quality and optimize finishing force control in the machining of Ti alloys. Barman et al. [23] introduced an innovative MRF tool for nano-finishing a bio-titanium alloy, achieving an initial surface roughness of 120 nm after a meticulous 6.3-hour process, ultimately resulting in a final surface roughness of 10 nm. Concurrently, Parameswari et al. [24] engineered a machining tool to refine flat Ti-6Al-4V discs, attaining a minimal surface roughness of 95 nm from an initial 400 nm within a 30-minute machining interval, as indicated by experimental studies. Despite considerable

advancements, practical challenges persist. In the traditional MRF process, the deformation and wear of the magnetic brush pose significant hurdles, adversely impacting the sustainability of the machining process. To address these challenges, researchers have redirected their focus toward magnetic abrasive machining, capitalizing on the adaptability and reproducibility of abrasive suspensions [25–27], aiming to optimize performance and circulation in the machining of titanium alloys. The findings underscore a notable improvement in the quality of the internal surface, as demonstrated by Kang et al. [28], who applied MRF to machine tubular curved surfaces. This advancement has spurred extensive discussions and further research in the field. While previous studies have successfully identified key parameters influencing the MRF process and bolstered its efficiency, challenges persist in its practical application. The performance of the magnetic brush emerges as a pivotal factor in the finishing process. In traditional MRF processing, the magnetic brush's effectiveness is hampered by limitations on the number and fixed position of abrasive particles within it. This constraint results in the gradual dulling of the abrasive particles' cutting edges, leading to diminished finishing efficiency as the process advances. Concurrently, the original structure of the magnetic brush undergoes deformation due to interaction with the workpiece, negatively impacting the precision of MRF processing. These challenges necessitate frequent replacements of the magnetic brush, limiting the duration of continuous magnetic finishing processes.

Beyond contemporary approaches aimed at optimizing the effectiveness of magnetic polishing during machining, researchers continually explore the utilization of permanent magnets to generate a magnetic field influencing the machining area. The advantages offered by permanent magnets, such as their compact size, portability, and independence from an external power source, make them particularly attractive. Various configurations of permanent magnets, including circular Halbach arrays, are under scrutiny to fine-tune the magnetic field precisely at the machining site [29, 30]. The cylindrical structure of the circular Halbach array is characterized by magnets arranged at an angle twice that of its centre, resulting in the creation of a robust and uniform magnetic field inside or outside the cylinder. Notably, this design has found applications in devices such as magnetic resonance imaging (MRI), nuclear magnetic resonance (NMR) [31, 32], and magnetic cooling, as documented in existing literature. Furthermore, investigations into the arrangement, and application [33, 34] of magnets, particularly in hollow planes and spheres, along with their integration with Halbach arrays, present novel avenues for advancing the efficiency of machining processes.

To address the challenges above, this paper proposes a novel MRF process featuring regenerated abrasive particles facilitated by a conveyor belt. In this innovative approach, the established MRF mixture is propelled by the conveyor belt, enabling the strip MRF slurry to move seamlessly along with it. Simultaneously, the MRF slurry engaged in polishing in the workpiece surface area undergoes continuous circulation and renewal. This dynamic process ensures the steadfastness of the MRF polishing procedure, eliminating the need for interruptions. Notably, issues related to the blunting of cutting edges on abrasive particles and deformation of the MRF ribbon during finishing can be circumvented. In contrast to conventional MRF methods, this proposed approach significantly enhances the uniformity of the finished surface and augments finishing efficiency. Moreover, to further elevate the magnetic field strength, a circular Halbach array is incorporated, working with the continuous

circulation of magnetic fluid through the conveyor belt. This integrated system is designed to generate a more robust magnetic field, providing an advanced solution for improving both surface quality and efficiency in the MRF process. The overarching objective is to conduct a thorough investigation and refinement of the MRF polishing process. The research systematically explores the impact of varying distributions of magnetic abrasive fluids on the conveyor belt on machining characteristics. To validate theoretical insights, a series of experiments were conducted to assess the feasibility of machining Ti-6Al-4V alloy through this innovative process. The study pays particular attention to the characteristics of a circular Halbach array for MRF with the regenerative magnetic abrasive stream. Moreover, it investigates the impact of crucial machining parameters, including working distance, abrasive and magnetism grain size on the observed alterations during the machining of Ti-6Al-4V workpieces. This comprehensive examination aims to advance our understanding of the intricacies involved in the magnetic polishing process and optimize its efficiency.

2. PRINCIPLE OF MAGNETO-RHEOLOGICAL FINISHING PROCESS WITH CIRCULAR HALBACH ARRAY WITH REGENERATIVE ABRASIVES

Figure 1 delineates the magnetic polishing process utilizing a Halbach array with magnetic abrasives within a circulating system. In the Magneto-Rheological Finishing (MRF) polishing procedure, the proposed magnetic slurry comprising Fe_3O_4 magnetic iron powder, demagnetized water and SiO_2 abrasive particles, is employed to transform the magnetic abrasive fluid into a slurry state, thereby fashioning a versatile and eco-friendly MRF polishing tool. This process is dichotomized into two primary segments: the driving component and the fluid circulation module. The driving segment predominantly encompasses the polishing wheel with a circular Halbach array, the belt tensioning wheel, the conveyor belt and the transmission wheel. Conversely, the fluid circulates section dedicated to the retrieval of MRF post-polishing, its storage, and the replenishment of the magnetic abrasive fluid. The driving wheel imparts energy to the conveyor belt, while the belt tensioner assumes the role of maintaining optimal belt tension during MRF polishing procedures.

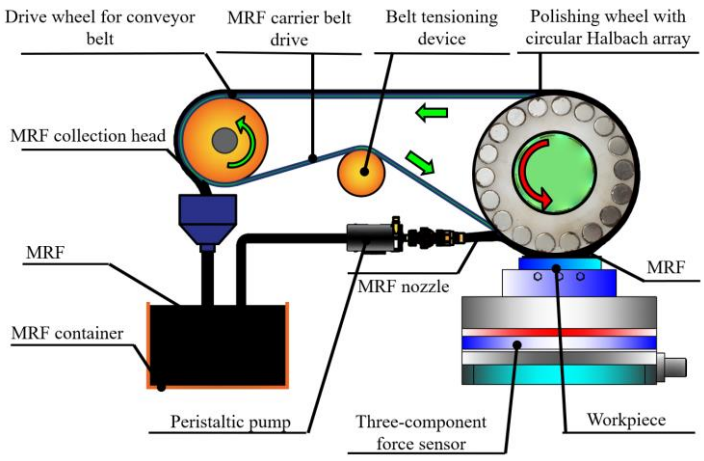

Fig. 1. Image experiment equipment by MRF polishing

Magnetic polishing wheels equipped with circular Halbach arrays deliver the magnetic abrasive fluid, which is introduced into the machining area via the conveyor belt. The circulating conveyor is tasked with transporting the magnetic abrasive fluids and facilitating the circulation of abrasive particles, thus facilitating a range of diverse machining steps. As shown in Fig. 2 illustrates the MRF polishing configuration employing circular Halbach arrays and regenerative abrasives.

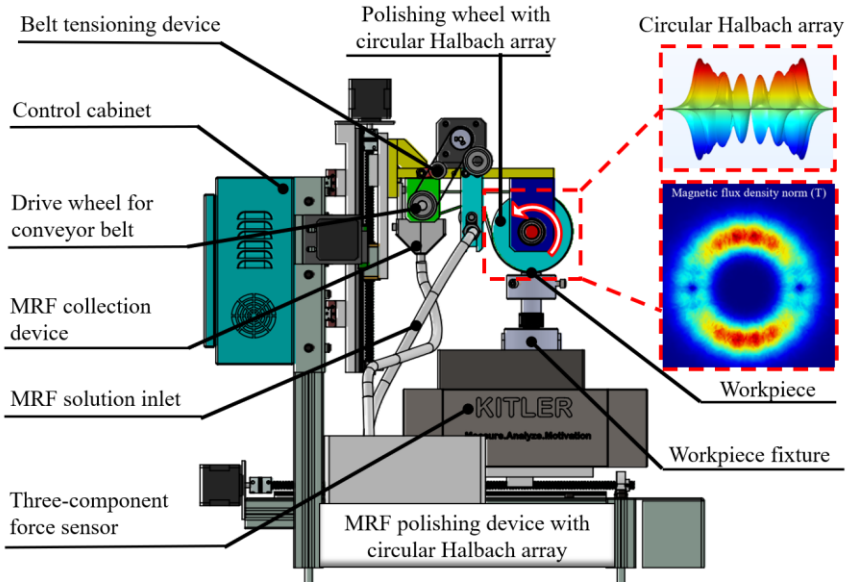

Fig. 2. Illustrates a diagram of the experimental equipment

In Figure 3, a cross-sectional view of the polishing wheel equipped with a circular Halbach array is presented. The circular Halbach array is crafted from Nd-Fe-B and boasts an outer diameter of 100 mm, a magnet length of 20 mm, and a diameter of 8 mm. The North and South poles of the magnetic ring are represented by different colours as depicted in Fig. 3. Magnets within the Halbach array play a crucial role with positioned circularly and in proximity to the outer edge of the plastic disk. Specifically, the circular Halbach array generates a magnetic field characterized by substantial impact force and a focused direction of impact towards the exterior of the conveyor belt.

In Figure 3, the depicted green lines represent magnetic induction line, delineating the trajectories along which magnetic particles will be attracted and mobilized. Within the machining zone, particles undergo the influence of forces F_X and F_Y directed along the magnetic force lines with x, y directions. These forces represent the magnetic force components exerted on the magnetic particles situated on the conveyor belt. Their expression is articulated by the following equation:

$$F_X = \mu_0 \times \chi \times V \times H \left[\frac{\partial H}{\partial x} \right] \tag{1}$$

$$F_Y = \mu_0 \times \chi \times V \times H \left[\frac{\partial H}{\partial y} \right] \tag{2}$$

in this context, V represents the volume of the magnetic particle, χ denotes the magnetic susceptibility of the magnetic particle, H and μ_0 magnetic field density and vacuum magnetic permeability. The gradient in the x, y direction is determined by $\frac{\partial H}{\partial x}$, $\frac{\partial H}{\partial y}$. Figure 3 depicts the magnetic force acting on magnetic particles with the formula as described below:

$$F = F_X \times \sin(\gamma_i) + F_Y \times \cos(\gamma_i) \tag{3}$$

in this equation, γ_i tilt angle of the magnetic induction line. The magnetic force is determined by F_M with mathematically expressed as follows:

$$F_M = \frac{3}{2}\mu_0 \times (\pi R^2) \times \left(\frac{X_R{}^2 H^2}{(3+X_R)^2} \right) \tag{4}$$

in this context, R represents the radius of the magnetic particle, XR is the specific susceptibility of the magnetic particle, and $m0$ is the magnetic permeability of the vacuum. Through the interaction between the magnetic particles and the magnetic field force, the MRF slurry will adhere tightly to the belt and move in the direction of the belt's movement, serving as tools to complete the machining process, as illustrated in Fig. 3.

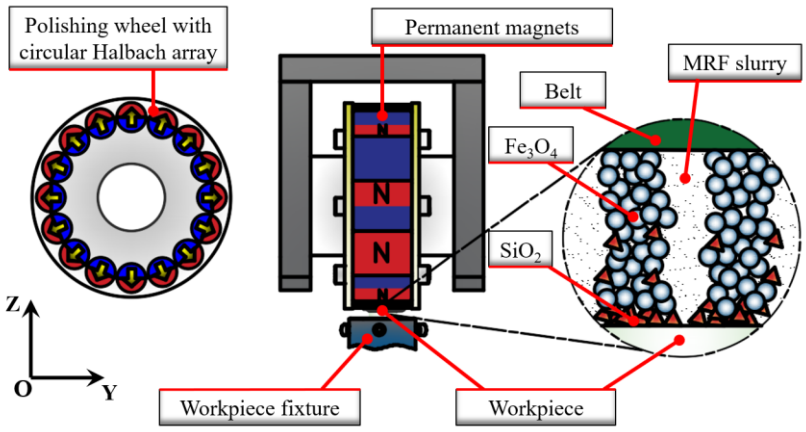

Fig. 3. Illustrates the polishing model featuring a Halbach array within the MRF polishing area

Throughout the MRF polishing process, the polishing wheel equipped with the Halbach array rotates as illustrated in Fig. 1. The magnetic abrasive fluid beneath the wheel is reclaimed at the end of each polishing cycle. As the MRF fluid advances towards the circular Halbach magnetic field array, with the established polishing distance, it undergoes a transition into a slurry state. Guided by the magnetic field, the magnetic abrasive fluid maintains a semi-solid state and is propelled upward to the top of the polishing wheel with the circular Halbach array. The conveyor belt persists in its motion, transporting the magnetic abrasive fluid to the recovery unit, where it is drawn into a reservoir. At this point, the magnetic abrasive fluid is no longer subject to the magnetic field and reverts to its liquid state, remaining in this state until it approaches the circular Halbach array wheel.

The magnetic abrasive fluid within the tank is pumped upward through the tube to the nozzle. With the established circular Halbach array the MRF solution from the nozzle is distributed and forms an MRF ribbon on the belt surface. The solid slurry state is quickly formed when an external magnetic force acts on the magnetic solution. In the subsequent stage, the magnetic abrasive fluid is transported by the conveyor belt to the lower region of the polishing wheel, positioning it within the material processing area. Following this, the magnetic abrasive fluid is expelled from the machining zone. This cyclical process capabilities aim to a magnetic abrasive fluid for material machining while ensuring a new continual supply of abrasive particles.

3. MAGNETIC FIELD ANALYSIS AND POLISHING FORCE WITH CIRCULAR HALBACH ARRAY

Simulation results of magnetic field intensity and magnetic field distribution on the Halbach array on the surface of the polishing wheel in cross-section are shown in Fig. 4. The visual representation in Fig. 4 aligns with the conveyor belt's width, specifically at the operational position corresponding to the lowest point of the polishing wheel. The conveyor belt width measures 18 mm, and the graphical representation of magnetic field intensity changes, as illustrated in Fig. 4, represents magnetic field strength in the polishing area. The demonstrations depict different magnetic field strengths in the *X* direction. Examining the graph reveals a substantial increase in magnetic field intensity within the range of 4 to 12 mm across the width of the measured surface.

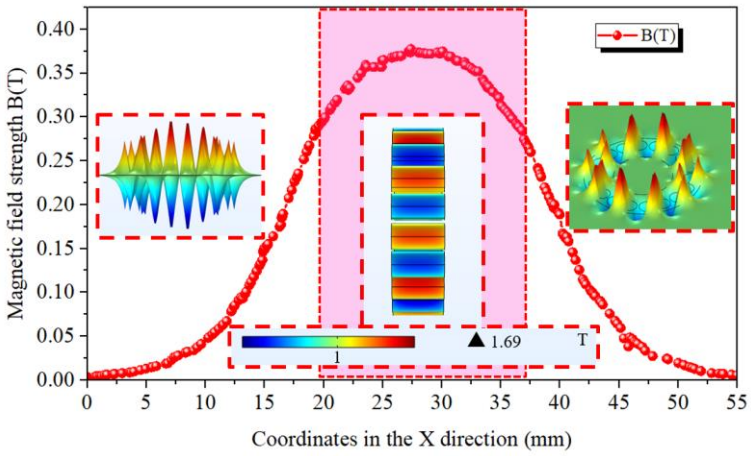

Fig. 4. Displays the results of magnetic field intensity analysis in the *X* direction

The analysis of magnetic field strength reveals notable variations between 10 and 20 mm and between 37 and 50 mm. As the system approaches the central region, the magnetic field intensity becomes more consistent, peaking at 0.375 T. The identified area with strong magnetic field intensity covers the belt's width, precisely 20 mm, influenced by the circular Halbach array acting on the conveyor belt. This results in a controlled flow of magnetic

abrasive fluid, sustaining a semi-solid state with heightened hardness within the effective width of the Halbach array applied to the conveyor belt or the polishing zone.

The simulation results are presented in Figs. 5a, 5b, and 5c offer a comprehensive analysis of the magnetic field intensity of the circular Halbach array across different perspectives: the coordinate plane perpendicular to the axis (OXZ plane), the axial cross-section, and the direction of the magnetic field vector aligned with the Halbach array. It is observed that the magnetic force is notably concentrated towards the outer region of the Halbach array. This concentration results in a robust magnetic force, enhancing its efficacy in various polishing processes. Notably, Fig. 5c provides valuable insights into the orientation of the magnetic field vector specifically in the context of the polishing wheel equipped with a circular Halbach array and conveyor belt. A closer examination of the right side reveals a distinct direction of the magnetic field vector on both sides of the conveyor belt and at the central position. The simulation illustrates that the magnetic field lines initiate from one side of the conveyor belt, run parallel to it in the middle, and then alter their course to move towards the opposite side of the conveyor belt. This aligns with the previously analysed magnetic field lines' effect. Specifically, the magnetic particles in the magnetic abrasive fluid organize into a dome structure, creating a magnetic chain region on the conveyor belt's surface under the influence of the magnetic field lines. This intricate process enhances the feasibility and effectiveness of the polishing operation.

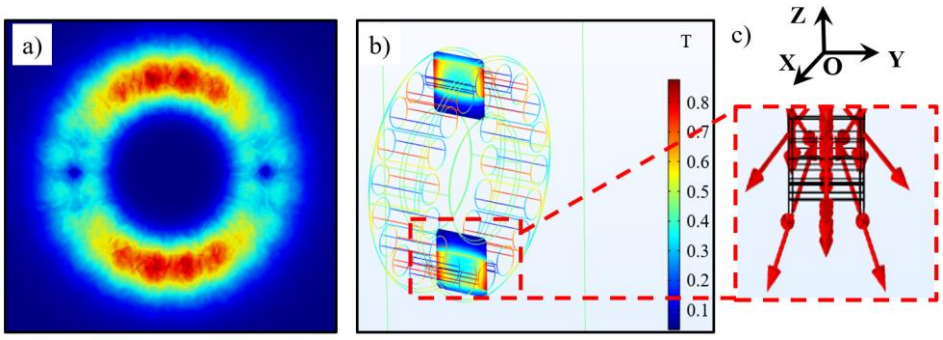

a) Simulation of the magnetic field intensity of a circular Halbach array in the Ozx coordinate plane

b) Simulate the magnetic field intensity in cross-section along the circular Halbach array axis

c) Magnetic field vector direction by Halbach array

Fig. 5. Simulation results of magnetic field vector direction with circular Halbach array

4. POLISHING FORCE BY CIRCULAR HALBACH ARRAY AND REGENERATIVE ABRASIVES

For a detailed investigation into the machining performance of the polishing wheel, the polishing force was continuously measured throughout the machining process. The schematic diagram of the force measurement system is depicted in Fig. 6. The tangential force (F_T) and normal force (F_N) components correspond to the F_X and F_Z forces obtained on the Kistler Type 9139AA three-component force measuring device. The force component in the Y direction is too small and therefore ignored in the polishing force analysis by the proposed model. The precise measurement conditions are outlined in Table 1.

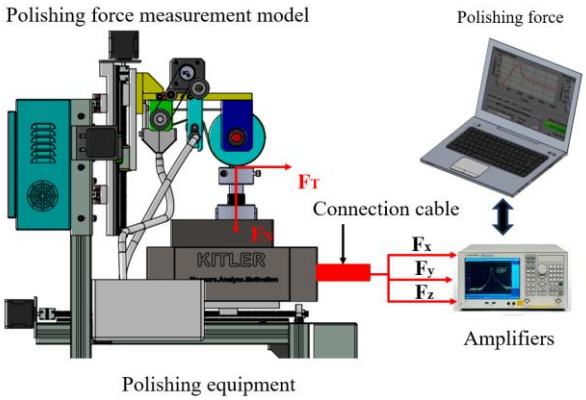

Fig. 6. The polishing force measurement system

Table 1. Conditions for measuring polishing force

Numerical order	Characteristic	Parameter	Unit
1	Polishing distance	0.1, 0.2	mm
2	Magnetic particles (Fe_3O_4)	Diameter 3	μm
3	Abrasive particles (SiO_2)	Diameter 1	μm
4	Belt drive motor speed	60	rpm
5	MRF flow from peristaltic pump	20	ml/min
6	Workpieces	Ti-6Al-4V	ϕ12×20 mm

The influence of the polishing distance on the polishing force has been investigated in this research. In Fig. 7, the results of force measurements corresponding to F_N and F_T on the Ti-6Al-4V workpiece with polishing distance 0.1 mm are presented.

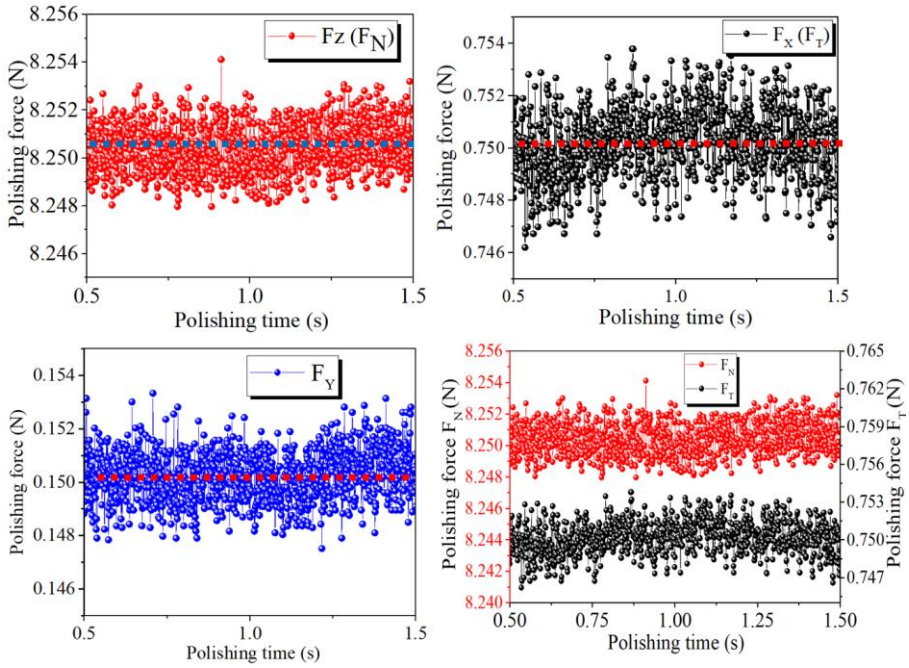

Fig. 7. Force measurement results

The force value obtained is determined by the average value with a straight horizontal line as shown in Fig. 8. The outcomes reveal that, as the polishing distance increases, the polishing force decreases. This phenomenon stems from the unique interplay of the polishing wheel's roles helps the magnetic fluid exert pressure on the workpiece by changing the state of the MRF fluid to a semi-solid state and attaching it tightly to the belt. As the polishing gap diminishes, this process induces pressure on the workpiece.

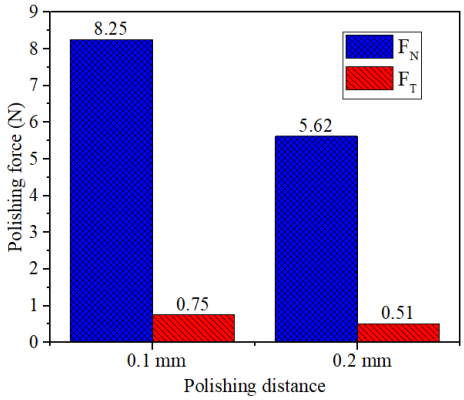

Fig. 8. Force measurement results with different polishing distances

5. EXPERIMENTAL SETUP

Figure 9 illustrates the configuration of the experimental setup. A Ti-6Al-4V workpiece, measuring 12 mm in diameter and 20 mm in height, was selected as the machining material. Utilizing the workpiece motor, rotational movement around its axis is achievable, in conjunction with the machine table equipped with a Kistler force measurement device capable of adjusting its coordinates along the *X* direction.

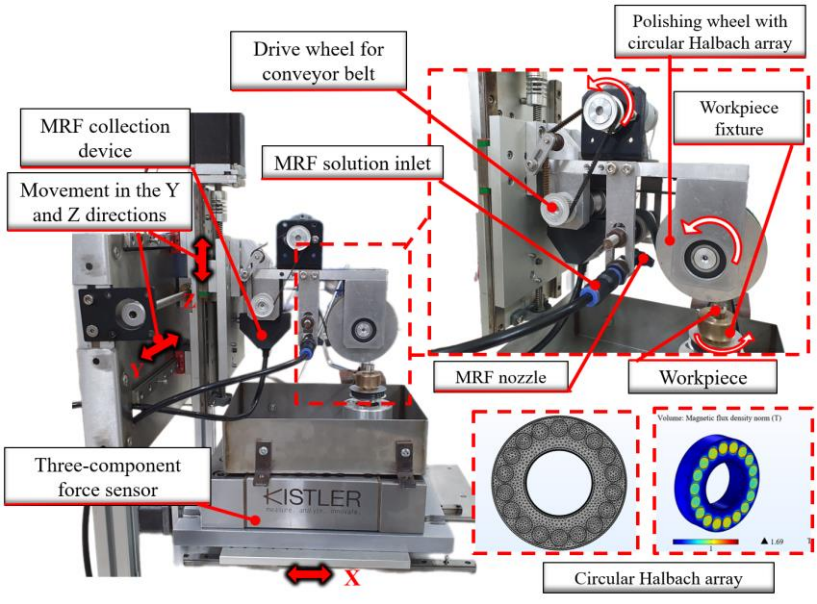

Fig. 9. External View of the Experimental Setup

This research aims to assess the impact of magnetic particle size, working gap, and abrasive particles on the polishing process. Magnetic liquid solution formulated from Fe_3O_4 magnetic particles averaging about 3 μm in diameter and magnetic iron particles with a diameter of 20 μm. Notably, both Fe_3O_4 and carbonyl iron powder are acknowledged as soft magnetic materials with exceptional magnetic properties. The resulting magnetic abrasive fluid maintains a consistent viscosity. Consequently, when subjected to a magnetic field, these particles can self-arrange along the magnetic induction lines. This creates optimal conditions for the magnetic abrasive fluid to transition from a liquid to a semi-solid slurry state efficiently. We conduct periodic workpiece measurements throughout the polishing process to track material changes that finish over time. The roughness measurements were derived by averaging results from two repeated polishing sessions conducted under identical conditions and at three distinct measuring positions on the workpiece surface after each polishing procedure. This methodology ensures a comprehensive assessment of surface quality. Additionally, the experimental design adheres to statistical principles, employing a sequential modification of technological parameters during the polishing process while maintaining other variables at a constant level. This statistical approach enhances the robustness of the experimental framework and contributes to the reliability and validity of the obtained results. At 10-minute intervals, we supplement the machining process by adding 1 ml of milling fluid to compensate for any losses.

6. RESULTS AND DISCUSSION

A crucial component within magnetic abrasive fluids comprises Fe_3O_4 magnetic particles, serving as the foundation for altering the state of the magnetic abrasive under the influence of a magnetic field. Additionally, Fe_3O_4 iron oxide powder significantly influences the distribution of SiO_2 abrasive particles, playing a pivotal role in both force transmission and abrasive particles. Thus, the efficacy of Fe_3O_4 powder becomes instrumental in ensuring the efficiency and quality of the MRF polishing process. Employing a working clearance of 0.1 mm and an abrasive particle size of 1 μm, the experiment utilized Fe_3O_4 iron powder with an average diameter of 3 μm and carbonyl iron powder with an average diameter of 20 μm with experimental parameters as described in Table 2. Figure 10 illustrates the impact of magnetic particle size on the machined surface. When employing carbonyl iron powder with an average diameter of 20 μm, the workpiece's surface roughness swiftly decreased from 463.5 to 52.4 nm, indicating a prompt enhancement in surface roughness. In contrast, when using Fe_3O_4 iron powder with an average diameter of 3 μm, the workpiece's surface roughness decreased from 484 to 260.3 nm. However, achieving superior surface quality proved to be more challenging with carbonyl particles possessing a diameter of 20 μm.

In Fig. 11, the 3D surface topography of the Ti-6Al-4V workpiece is presented both before and after machining, and the measurements were conducted using the Zygo Corporation's NewView 7100 optical measurement system. Utilizing Fe_3O_4 iron powder with an average diameter of 20 μm induces a significant transformation in the original surface structure of the machining area, being replaced by the structure resulting from the machining process.

Table 2. Polishing conditions

Numerical order	Characteristic	Parameter	Unit
1	Polishing distance	0.1	mm
2	Magnetic particles (Fe_3O_4)	Diameter 3	µm
		Diameter 20	µm
3	Abrasive particles (SiO_2)	Diameter 1	µm
4	Belt drive motor speed	60	Rpm
5	MRF flow from peristaltic pump	20	ml/min
6	Workpieces	Ti-6Al-4V	ϕ12×20 mm
7	Polishing time	30	Min

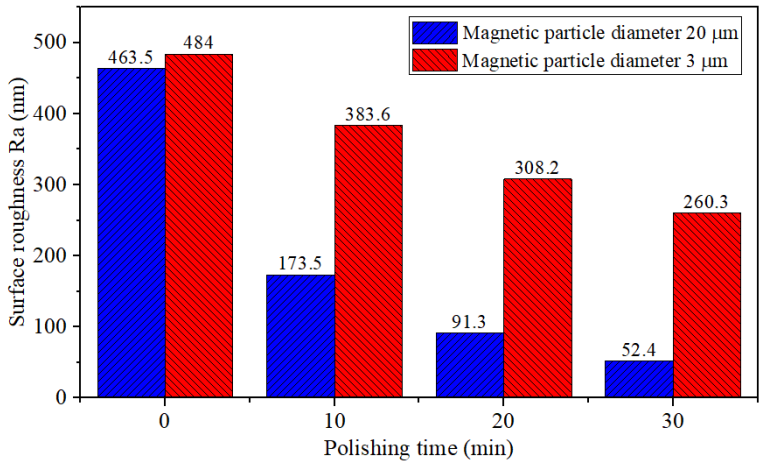

Fig. 10. Illustrates the impact of Fe_3O_4 magnetic particle size on surface roughness

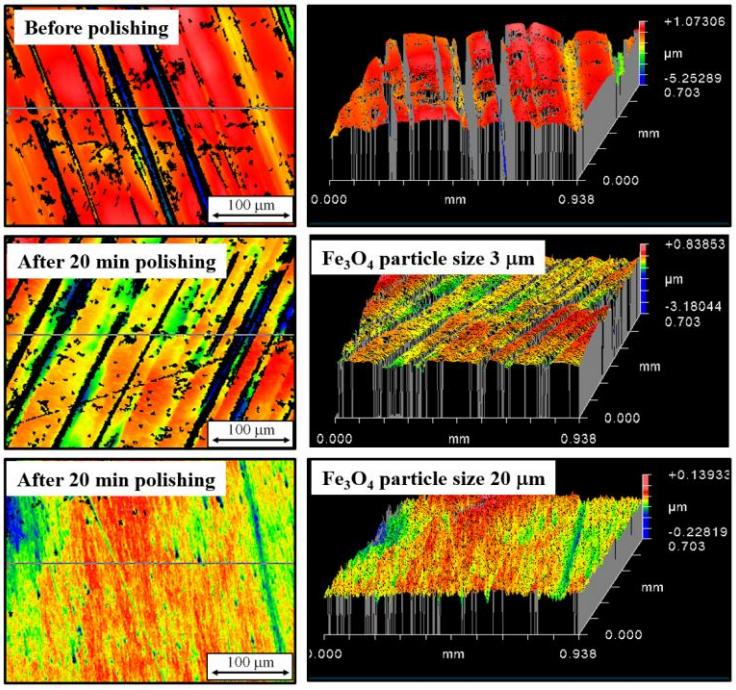

Fig. 11. 3D surface morphology when polished with different magnetic particle sizes

The orientation of the machining area structure becomes consistent, aligning with the motion direction of the magnetic abrasive fluid. In the case of Fe_3O_4 iron powder with an average diameter of 3 μm, the surface topography of the machined area improved compared to its initial state. Some deep grooves have been mitigated. Simultaneously, the undulations on the machined surface tend to decrease marginally. However, many deep grooves persist. Consequently, in the current experimental conditions, the utilization of Fe_3O_4 iron powder with an average diameter of 20 μm demonstrates superior effectiveness in enhancing the surface roughness of the Ti-6Al-4V workpiece compared to Fe_3O_4 iron powder with an average diameter of 3 μm.

With varying polishing distances, the enhancement in workpiece surface roughness is illustrated in Fig. 12 with experimental parameters as described in Table 3. For working gaps of 0.1, 0.2, and 0.3 mm, the surface roughness of the workpiece reduced from 448.4, 427.8, and 474.2 nm to 154.6, 64.2, and 48.3 nm, respectively. This outcome indicates that the most effective improvement in workpiece surface quality is attained with a working gap of 0.1 mm.

Table 3. Polishing conditions

Numerical order	Characteristic	Parameter	Unit
1	Polishing distance	0.1	mm
		0.2	mm
		0.3	mm
2	Magnetic particles (Fe_3O_4)	Diameter 20	μm
3	Abrasive particles (SiO_2)	Diameter 1	μm
4	Belt drive motor speed	60	Rpm
5	MRF flow from peristaltic pump	20	ml/min
6	Workpieces	Ti-6Al-4V	ϕ12×20 mm
7	Polishing time	30	Min

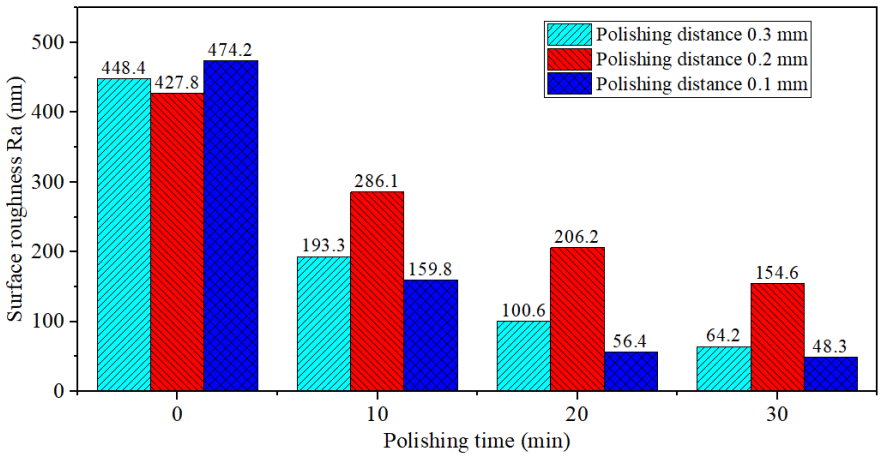

Fig. 12. Effect of polishing distance on surface roughness

To scrutinize the influence of abrasive particle sizes on workpiece surface roughness, the experiments were conducted following the specified procedure in Table 4. The polishing distance was maintained at 0.1 mm, using Fe_3O_4 iron powder with an average particle

diameter of 20 μm. To investigate the role of SiO_2 abrasive particle size on the efficiency of the polishing process and its effect on the final surface quality. In this study, we employed abrasive particles with increasing sizes, namely 1, 5, 10, and 20 μm. The outcomes of the respective polishing processes, as depicted in Fig. 13, reveal surface roughness values represented by Ra measurements of 39.6, 56.9, 83.8, and 135.2 nm, respectively. The experimental findings demonstrate a proportional increase in surface roughness with the enlargement of abrasive particle diameter. This correlation can be attributed to the challenge posed by larger abrasive particles in maintaining adequate buoyancy on the MRF surface during the polishing process, leading to a decreased presence of abrasive particles on the machined surface and subsequently reducing the efficiency of the machining process.

Moreover, the large size of non-magnetic abrasive particles hampers the creation of impactful magnetic forces acting on the abrasive particles, diminishing their polishing effects on the machined surface. The inadequacy of holding force from magnetic particles can cause aggregation of abrasive particles in specific areas, resulting in the distribution of abrasive particles in the MRF is not uniform and the creation of substantial scratches upon impact with the workpiece surface. This is exacerbated by the inherent nature of large-sized abrasive particles, which tend to produce rougher and deeper scratches compared to their smaller counterparts. Along with that, in MRF polishing, the abrasive particle needs to be correspondingly smaller than one-third the size of the magnetic particles to help the magnetic particles grip the abrasive particles tightly in the polishing processes [35]. This facilitates a more effective clamping force from the magnetic particles to the abrasive particles during polishing processes. In the conducted experiments, abrasive particles with a diameter ratio exceeding one-third of the magnetic abrasive particle diameter, exemplified by abrasive particles with diameters of 10 and 20 μm, exhibited restricted polishing efficacy. Conversely, smaller abrasive particles, specifically those with sizes of 1 and 5 μm, demonstrated superior polishing efficiency. Therefore, the recommendation is to opt for abrasive particles of smaller size, as indicated by the experimental results. This choice enhances the ability of abrasive particles to float more uniformly on the workpiece surface, coupled with a more effective clamping force from magnetic particles to abrasive particles, thereby improving overall polishing efficiency.

Table 4. Polishing conditions

Numerical order	Characteristic	Parameter	Unit
1	Polishing distance	0.1	mm
		0.2	mm
		0.3	mm
2	Magnetic particles (Fe_3O_4)	Diameter 20	μm
3	Abrasive particles (SiO_2)	Diameter 1	μm
	Abrasive particles (SiO_2)	Diameter 5	μm
	Abrasive particles (SiO_2)	Diameter 10	μm
	Abrasive particles (SiO_2)	Diameter 20	μm
4	Belt drive motor speed	60	rpm
5	MRF flow from peristaltic pump	20	ml/min
6	Workpieces	Ti-6Al-4V	ϕ12×20 mm
7	Polishing time	30	Min

The optimal machining efficiency is underscored when utilizing small abrasive particles corresponding to 1 μm. Moving forward, our subsequent study will delve into the realm of even nanometer-sized abrasive particles, with a specific focus on unravelling the role played by nanometer abrasive particles and nanometer magnetic particles in MRF polishing ability. This endeavour seeks to contribute further insights into the intricate dynamics of nanoscale abrasive applications, paving the way for advancements in polishing technology.

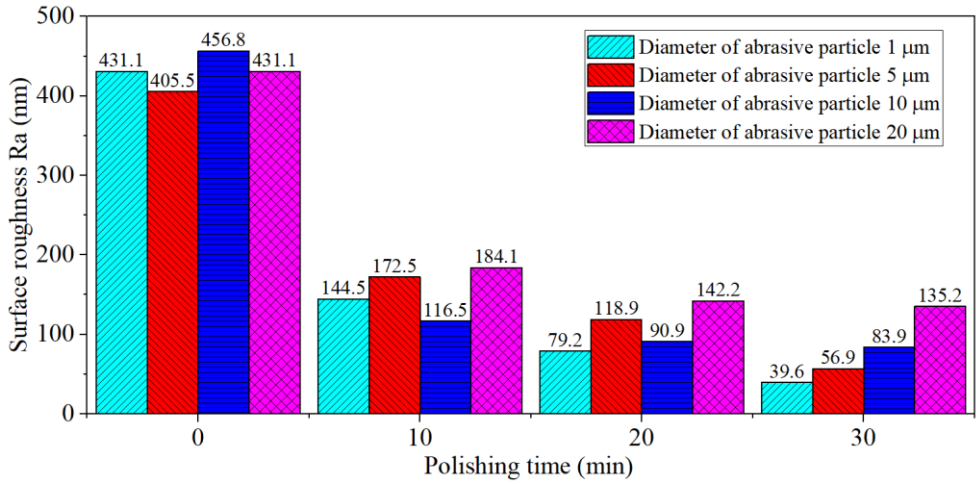

Fig. 13. Illustrates surface roughness according to diameter of abrasive particle

7. CONCLUSIONS

This research employed simulation and theoretical analysis methods to delve into the operational mechanism of magnetic abrasive fluid in the machining of Ti-6Al-4V workpieces using circular Halbach arrays and regenerative abrasives. A series of systematic experiments were carried out to assess the impact of varied distribution states of magnetic abrasive fluid on the machining process. The key findings of the study are outlined as follows:

- Narrowing the polishing gap results in a denser distribution of magnetic abrasive fluid on the conveyor belt, leading to an increased contact area during machining. This, in turn, contributes to a gradual rise in machining force and improved efficiency. Achieving a working gap as small as 0.1 mm produces a noticeably smoother final machined surface.
- Within the existing experimental parameters, Fe_3O_4 iron powder with an average diameter of 20 μm outperforms its 3 μm counterpart, yielding a superior final surface with enhanced smoothness and machining efficiency.
- The diameter of the abrasive particle 1 μm demonstrates optimal efficiency and machining quality.
- When employing a polishing gap is 0.1 mm, along with Fe_3O_4 magnetic grain featuring an average diameter of 20 μm and 1 μm SiO_2 abrasive particle, the surface roughness of the Ti-6Al-4V workpiece decreased from 431.1 to 39.6 nm within a 30-minute timeframe.

- In this current study, the experimental methodology focused on a sequential analysis of individual factors influencing surface roughness, lacking the incorporation of effective optimization mathematical tools. Furthermore, the assessment of surface roughness was solely based on the Ra metric, with no exploration into the material removal potential and costs associated with the proposed polishing process.
- To enhance the depth of insights, future research endeavours will broaden the scope to encompass diverse metrics. We aim to integrate comprehensive assessments that include not only surface roughness in Ra but also methodological considerations for determining surface roughness in Sa as well as material removal potential and associated costs. Additionally, forthcoming studies will delve into the impact of abrasive particle sizes and nanometric magnetic particles on polishing efficiency. By conducting these investigations, we aspire to provide a more holistic understanding and address vital aspects of the MRF polishing process.

ACKNOWLEDGEMENT

This work is financially supported by the Hanoi University of Industry (Grant No. DHCN:2023.06).

REFERENCES

[1] TIEN D.H., DUY T.N., THOA P.T.T., 2023, *Applying GPR-FGRA Hybrid Algorithm For Prediction and Optimization of Eco-Friendly Magnetorheological Finishing Ti–6Al–4V Alloy*, International Journal on Interactive Design and Manufacturing, 17/2, 729–745, https://doi.org/101007/s12008-022-00995-x.

[2] NGUYEN D., WU J., QUANG N.M., DUC L.A., SON P. X., 2021, *Applying Fuzzy Grey Relationship Analysis and Taguchi Method in Polishing Surfaces of Magnetic Materials by Using Magnetorheological Fluid*, The Inter. J. of Advanced Manufacturing Technology, 112/5, 1675–1689, https://doi.org/10.1007/s00170-020-06567-1.

[3] WANG B., TIE G., SHI F., ZHANG W., SONG C., GUO S., 2023, *Design and Frequency Control Study of Small-Sized Magnetorheological Finishing Device Applied in Optical Manufacturing*, Journal of Manufacturing Processes, 108, 863–876, https://doi.org/10.1016/j.jmapro.2023.11.031.

[4] GHOSH G., SIDPARA A., BANDYOPADHYAY P.P., 2023, *Performance Improvement of Magnetorheological Finishing Using Chemical Etchant and Diamond-Graphene Based Magnetic Abrasives*, Precision Engineering, 79, 221–235, https://doi.org/10.1016/j.precisioneng.2022.10.008.

[5] XU J., LI J., NIE M., LIU Y., 2023, *Material Removal Mechanism in Magnetorheological Foam Plane Finishing*, Journal of Manufacturing Processes, 87, 168–182, https://doi.org/10.1016/j.jmapro.2023.01.043.

[6] XIA Z., FANG F., AHEARNE E., TAO M., 2020, *Advances in Polishing of Optical Freeform Surfaces: a Review*, Journal of Materials Processing Technology, 286, 116828, https://doi.org/10.1016/j.jmatprotec.2020.116828.

[7] ZHAO F., et al., 2023, *Advanced Nonlinear Rheology Magnetorheological Finishing: A Review*, Chinese Journal of Aeronautics, https://doi.org/10.1016/j.cja.2023.06.006.

[8] CHEN Z., YAN Q., PAN J., LIAO Y., 2024, *Magnetization and Self-Sharpening Mechanism of Polymerized Diamond Abrasive Based on Magnetorheological Polishing Technology*, Diamond and Related Materials, 141, 110709, https://doi.org/10.1016/j.diamond.2023.110709.

[9] YU B., et al., 2023, *Surface Polishing of Cocrmo Alloy by Magnetorheological Polishing*, Surface and Coatings Technology, 475, 130162, https://doi.org/10.1016/j.surfcoat.2023.130162.

[10] HARRIS D., 2011, *History of Magnetorheological Finishing*, Proc SPIE, 8016, https://doi.org/10.1117/12.882557.

[11] XU D., HU T., 2023, *Modelling and Vibration Control of Magnetorheological-Based Polishing Tool for Robotic Polishing Process*, Mechanical Systems and Signal Processing, 195, https://doi.org/10.1016/j.ymssp.2023.110290.

[12] SHAFRIR S., et al., 2009, *Zirconia Coated Carbonyl Iron Particle-Based Magnetorheological Fluid For Polishing*, Applied Optics/ 48/35, 6797-6810, https://doi.org/10.1364/AO.48.006797.

[13] HOU Z., NIU X., LU Y., ZHANG Y., ZHU Y., 2021, *Effect of Zno-Sio2 Composite Abrasive on Sapphire Polishing Performance and Mechanism Analysis*, ECS J. Solid State Sci. Technol. 10, 104001.
[14] SHI X., PAN G., ZHOU Y., XU L., ZOU C., GONG H., 2015, *A Study of Chemical Products Formed on Sapphire (0001) During Chemical–Mechanical Polishing*, Surface and Coatings Technology, 270, 206–220, https://doi.org/10.1016/j.surfcoat.2015.02.053.
[15] MA J., XU N., LUO Y., LIN Y., PU Y., 2023, *Enhancing the Polishing Efficiency of CeO_2 Abrasives on the SiO_2 Substrates by Improving the Ce^{3+} Concentration on Their Surface*, ACS Applied Electronic Materials, 5/1, 526–536, https://doi.org/10.1021/acsaelm.2c01553.
[16] PAN J., CHEN Z., YAN Q., 2020, *Study on the Rheological Properties and Polishing Properties of Sio2@CI Composite Particle for Sapphire Wafer*, Smart Materials and Structures, 29, 11, 114003, https://doi.org/10.1088/1361-665X/abb21c.
[17] ZHAI Q., ZHAI W., DENG T., 2023, *Study on Process Optimization of Ultrasound Assisted Magneto-Rheological Polishing of Sapphire Hemisphere Surface Based on Fe_3O_4/SiO_2 Core-Shell Abrasive*s, Tribology International, 181, 108318, https://doi.org/10.1016/j.triboint.2023.108318.
[18] QUANG N.M. et al., 2023, *A New Environmentally Friendly* Chemical Mechanical *Polishing Method Applied for Surface Finishing Ti-6Al-4V Allo*y, J. of Mach. Eng., 23/4, 64-76 https://doi.org/10.36897/ jme/169614.
[19] ZHA X., QIN H., YUAN Z., XI L., ZHANG T., JIANG F., 2023, *Effect of Cutting Feed Rate on Machining Performance and Surface Integrity in Cutting Process of Ti-6Al-4V Alloy*, The International Journal of Advanced Manufacturing Technology, 1–19, https://doi.org/10.1007/s00170-023-12458-y.
[20] WANG J., et al., 2023, *Surface Polishing and Modification of Ti-6Al-4V Alloy by Shear Thickening Polishing*, Surface and Coatings Technology, 468, 129771, https://doi.org/10.1016/j.surfcoat.2023.129771.
[21] PRIYANKA C.P., KRISHNAN K., KEERTHI SUDEEP U., RAMACHANDRAN K.K., 2023, *Osteogenic and Antibacterial Properties of Tin-Ag Coated Ti-6Al-4V Bioimplants with Polished and Laser Textured Surface Topography*, Surface and Coatings Technology, 474, 130058, https://doi.org/10.1016/j.surfcoat.2023.130058.
[22] WANG J., et al., 2021, *Chemistry Enhanced Shear Thickening Polishing of Ti–6Al–4V*, Precision Engineering, 72, 59–68, https://doi.org/10.1016/j.precisioneng.2021.04.002.
[23] BARMAN A., DAS M., 2017, *Nano-Finishing of Bio-Titanium Alloy to Generate Different Surface Morphologies by Changing Magnetorheological Polishing Fluid Compositions*, Precision Engineering, 51, 145–152 https://doi.org/10.1016/j.precisioneng.2017.08.003.
[24] PARAMESWARI G., JAIN V., RAMKUMAR J., NAGDEVE L., 2019, *Experimental Investigations into Nanofinishing of Ti6Al4V Flat Disc Using Magnetorheological Finishing Process*, The International Journal of Advanced Manufacturing Technology, 100, 155–165, https://doi.org/10.1007/s00170-017-1191-3.
[25] XU J., ZOU Y., XIE H., *Investigation on the Finishing Characteristics of a Magnetic Abrasive Finishing Process with Magnetic Abrasive Slurry Circulation System*, Machines, 9/9, https://doi.org/10.3390/Machines9090195.
[26] ZOU Y., SATOU R., YAMAZAKI O., XIE H., *Development of a New Finishing Process Combining a Fixed Abrasive Polishing with Magnetic Abrasive Finishing Process*, Machines, 9/4, https://doi.org/10.3390/Machines 9040081.
[27] YUAN Y., ZHAO X., YOU K., YIN X., 2023, *Research on an Epoxy Resin Magnetoelastic Abrasive: Application in Tool Edge Preparation*, Proceedings of the Institution of Mechanical Engineers, Part B: Journal of Engineering Manufacture, P. 09544054231205100, https://doi.org/10.1177/09544054231205100.
[28] KANG YAMAGUCHI J.H., 2012, *Internal Finishing of Capillary Tubes by Magnetic Abrasive Finishing Using A Multiple Pole-Tip System*, Prec. Eng., 36/3, 510–516, https://doi.org/10.1016/j.precisioneng.2012.01.006.
[29] MAAMER B., TOUNSI F., KAZIZ S., JAZIRI N., BOUGHAMOURA A., 2022, *A Halbach Cylinder-Based System for Energy Harvesting from Rotational Motion with High Power Density*, Sensors and Actuators A: Physical, 337, 113428, https://doi.org/10.1016/j.sna.2022.113428.
[30] LEE J., NOMURA T., DEDE E.M., 2017, *Topology Optimization of Halbach Magnet Arrays Using Isoparametric Projection*, J. of Magnetism and Magnetic Materials, 432, 140–153, https://doi.org/10.1016/j.jmmm.2017.01.092.
[31] CHANG W.-H., CHEN J.-H., HWANG L.-P., 2006, *Single-Sided Mobile NMR with a Halbach Magnet, Magnetic Resonance Imaging*, 24/8, 1095–1102, https://doi.org/10.1016/j.mri.2006.04.005.
[32] YU P., et al., 2022, *Theoretical Foundation for Designing Multilayer Halbach Array Magnets For Benchtop NMR and MRI*, Journal of Magnetic Resonance, 344, 107322, https://doi.org/10.1016/j.jmr.2022.107322.
[33] MASI J., 2013, *Overview of Halbach Magnets and their Applications,* Electrical Manufacturing and Coil Winding Expo 2010–2013, 134–139.
[34] ANJUM Z., VAITHLINGAM A., SULAIMAN E., SHAHRUKH D., 2016, *Application of Halbach Magnet Array in Designing a Permanent Magnet Synchronous Machine*, IJCTA, 9/6, 2835–2842.
[35] WANG Y., WU Y., NOMURA M., 2017, *Fundamental Investigation on* Nano-Precision *Surface Finishing of Electroless Ni–P-Plated STAVAX Steel Using Magnetic* Compound Fluid Slurry, Precision Engineering, 48, 32–44, https://doi.org/10.1016/j.precisioneng.2016.11.003.